CONSIDERATION OF PORE FORMATION AT ESTIMATION OF LIMITING STATE IN ZONE OF PRESSURE VESSEL WALL THINNING DEFECT

V.I. MAKHNENKO, E.A. VELIKOIVANENKO, G.F. ROZYNKA and **N.I. PIVTORAK**
E.O. Paton Electric Welding Institute, NASU, Kiev, Ukraine

The tough fracture models allowing for pores forming in plastic flow either at non-metallic inclusions or in matrix from the microcracks that do not propagate by cleavage mechanism provide for the corresponding algorithms of growth of the pore due to plastic strains and respective redistribution of the stress-strain state. At present, the interest in these models is determined by growth of the scope of prediction and expert estimates for the welded structures, based on calculation estimation of the limiting state. In a number of cases, in view of the trend to utilization of high-strength and sufficiently ductile materials in the welded structures, the limiting state occurs under the tough deformation conditions at the rigid stressed state, which contribute to the pore formation. Fracture as a result takes place at relatively small plastic strains that rapidly reduce deformation capacity of corresponding welded assemblies before fracture.

Keywords: *steel pressure vessels, development of plastic flow, limiting state, pore formation, fracture zone, criteria of fracture involving pores, spontaneous fracture*

Operational defects of wall thinning in current welded pressure vessels are the most widely identified defects of long-term service structures (main pipeline, oil and gas storages, tank cars etc.). At periodic technical diagnostics of such structures the identified defects are estimated from point of view of safe operation of the structure for a period at least up to the next technical diagnostics. Specific rules based on corresponding calculation and experimental investigations are applied at that. These rules are improved according to accumulation of facts of their application, change of operation conditions for specific type of structures, development of calculation models of loading (fracture) as well as methods of realization of these models.

Observed significant progress in computer engineering, deformation and fracture mechanics of structural materials, respectively, provides for realization of the more complex physical models. It is a good basis for development of more detailed models of behavior of structural material at deformation (in stage close to fracture) as well as at fracture to certain extent. This makes the calculation approaches to prediction of a limiting state for complex cases of deformation sufficiently suitable to that is observed in experiment allowing reducing the scope of expensive experiments. Such an approach is connected with attraction of additional physical and mathematical models for development of information related with the coming of limiting state. Work in this direction is actively performed in different countries. Works of scientists of Siberian school of Prof. V.E. Panin in scope of new scientific direction, i.e. physical mesomechanics of materials [1], are worthy of notice among the current investigations. Deformation of material on mesolevel, i.e. considering significant physical discontinuity determined by presence of different interfaces (for example, gain boundary) with further estimation of reaction of material on macrolevel by means of average of characteristics of stress-strain state along representative mesovolume is considered in scope of this direction. Primitive example of inelastic material behavior according to [1] is a «shear + rotation» that allows preserving continuity condition up to fracture. The latter is a final stage of material fragmentation on macrolevel when global shear buckling takes place.

Pore formation in many cases is an important phase of material deformation before fracture stage. The pores are formed in plastic flow at non-metallic inclusions or in matrix from the microcracks that do not propagate by cleavage mechanism, i.e. being almost essential attribute of material tough fracture. It is not surprising that a great attention is paid to the issue of formation and growth of pores at tough fracture of materials [2–4]. Initial dimensions of appearing pores are not large around 1 μm as a rule. Therefore, their influence on deformation processes and fracture can be considered in scope of mesolevel models, i.e. corresponding inhomogeneity of material properties in pore volumes and out of these volumes.

The results obtained under the following assumptions are given below.

The pores are nucleated in an arbitrary finite element (structural volume) under isothermic conditions, when intensity of plastic strain ε_i^p is more than specified value $(\varepsilon_i^p)_\mathrm{n}$ and they are uniformly distributed along the element volume, i.e. concentration of pores per unit of element volume is

$$\begin{gathered}\rho_V = \frac{V_\mathrm{p}}{V_\mathrm{f.e}} \text{ at } \varepsilon_i^p \ge (\varepsilon_i^p)_\mathrm{n}, \\ \rho_V = 0 \text{ at } \varepsilon_i^p < (\varepsilon_i^p)_\mathrm{n},\end{gathered} \tag{1}$$

where V_p is the pore volume; $V_\mathrm{f.e}$ is the element volume without pores.

ρ_S concept of pore concentration per unit of sectional area of the element (that can be observed in sample fracture) is introduced. By analogy with (1)

$$\begin{gathered}\rho_S = \frac{S_\mathrm{p}}{S_\mathrm{f.e}} > 0 \text{ at } \varepsilon_i^p \ge (\varepsilon_i^p)_\mathrm{n}, \\ \rho_S = 0 \text{ at } \varepsilon_i^p < (\varepsilon_i^p)_\mathrm{n},\end{gathered} \tag{2}$$

where S_p is the area of pores in given section of $S_\mathrm{f.e}$ value.

l_p is the total length of pores per unit of linear dimension $l_\mathrm{f.e}$, respectively. Then

$$\rho_l = \frac{l_\mathrm{p}}{l_\mathrm{f.e}}. \tag{3}$$

Relationship between ρ_V and ρ_l is

$$\rho_V = (1 + \rho_l)^3 - 1 = 3\rho_l \left(1 + \rho_l + \frac{1}{3}\rho_l^2\right) \approx 3\rho_l. \tag{4}$$

Correspondingly $\rho_S = 2\rho_l \left(1 + \frac{1}{2}\rho_l\right) \approx 2\rho_l$.

Developed plastic flow promotes growth of pore linear dimensions according to Rice–Tracy law [4] at $\varepsilon_i^p \ge (\varepsilon_i^p)_\mathrm{n}$.

Assume that the amount of pores in given structural volume has little changes, but their dimensions increase:

$$\frac{dl}{d\varepsilon_i^p} = 0.28 l \exp\left(1.5\,\frac{\sigma_m}{\sigma_i}\right), \tag{5}$$

where σ_m/σ_i is the rigidity of stressed state; $\sigma_m = \frac{1}{3}(\sigma_{rr} + \sigma_{\beta\beta} + \sigma_{zz})$ is the average normal stress in coordinate system r, β, z;

$$\begin{gathered}\sigma_i = \frac{1}{\sqrt{2}}\,[(\sigma_{rr} - \sigma_{\beta\beta})^2 + (\sigma_{rr} - \sigma_{zz})^2 + \\ + (\sigma_{\beta\beta} - \sigma_{zz})^2 + 6(\sigma_{rz}^2 + \sigma_{r\beta}^2 + \sigma_{\beta z}^2)]^{1/2}\end{gathered} \tag{6}$$

is the stress intensity;

$$\begin{gathered}d\varepsilon_i^p = \frac{\sqrt{2}}{3}\,[(d\varepsilon_{rr}^p - d\varepsilon_{\beta\beta}^p)^2 + (d\varepsilon_{rr}^p - d\varepsilon_{zz}^p)^2 + \\ + (d\varepsilon_{\beta\beta}^p - d\varepsilon_{rr}^p)^2 + 6(d\varepsilon_{r\beta}^p)^2 + 6(d\varepsilon_{rz}^p)^2 + 6(d\varepsilon_{\beta z}^p)^2]^{1/2}\end{gathered}$$

is the intensity of increase of plastic strain.

Under mentioned above assumption that amount of pores in given volume V_0 has small changes, the change of ρ_l value corresponds with relative variation of the linear dimensions due to porosity.

Respectively, equation of relationship of strain tensor $d\varepsilon_{ij}$ and stress tensor σ_{ij} at i, $j = r$, z, β allowing for linear elongation equals ρ_l can be written in the following way:

$$\begin{gathered}d\varepsilon_{ij} = d\left(\frac{\sigma_{ij} - \delta_{ij}\sigma_m}{2G}\right) + \\ + d\lambda(\sigma_{ij} - \delta_{ij}\sigma_m) + \delta_{ij}[d(K\sigma_m) + d\rho_l],\end{gathered} \tag{7}$$

where ρ_l is the solution of equation (5) at $l = \rho_l$ and initial ρ_l value on (1) and (4); $G = E/(2(1 + \nu))$; $K = (1-2\nu)/E$; E is the Young's modulus; ν is the Poisson's ratio; $\delta_{ij} = 1$ at $i = j$ and $\delta_{ij} = 0$ at $i \ne j$.

Under sequential tracing of development of plastic strain and initial value of ρ_V^init in moment $k = 0$ on (1), assuming that $d\varepsilon_i^p$ value has small changes in a course of tracing steps k-th and $k + 1$st, solution of equation (5) relatively to value ρ_l will give

$$\ln \frac{\rho_l^{(k+1)}}{\rho_l^{(k)}} = 0.28 \exp\left(1.5\,\frac{\sigma_m^{(k)}}{\sigma_i^{(k)}}\right)(\Delta\varepsilon_i^p)^{(k)}. \tag{8}$$

Under values of relationship $x = \frac{\rho_l^{(k+1)}}{\rho_l^{(k)}}$ close to one, expanding $\ln x$ as a power series

$$\ln x = 2\sum_{n=1}^{\infty}\left(\frac{x-1}{x+1}\right)^n \frac{1}{n} \tag{9}$$

and being limited by member $n = 1$, the following will be obtained:

$$\begin{gathered}\rho_l^{(k+1)} = \frac{(2 + A_k)\rho_l^{(k)}}{2 - A_k}, \text{ where} \\ A_k = 0.28 \exp\left(1.5\,\frac{\sigma_m^{(k)}}{\sigma_i^{(k)}}\right)(\Delta\varepsilon_i^p)^{(k)}\end{gathered} \tag{10}$$

starting from $k = 0$, for which $\rho_l^{(0)}$ is determined by conditions (4).

Knowing $\rho_l^{(k)}$ ($k = 0, 1, 2, \dots$), an increment of elongation of linear dimensions of given finite element due to porosity will be found for (7)

$$\Delta\rho_l^{(k+1)} = \rho_l^{(k+1)} - \rho_l^{(k)} = \rho_l^{(k)} \frac{A_k}{1 - 0.5A_k} \qquad (11)$$
$$(k = 0, 1, 2, \dots).$$

It follows from mentioned above that consideration of porosity affects to certain extent the strain and stress fields due to additional volumetric changes of $\Delta\rho_l^{(k+1)}$ ($k = 0, 1, 2, \dots$) value similar to such at temperature expansion $\Delta\varphi$ [5].

Besides, realization of flow conditions and criteria of limiting state requires consideration of net-stress in sections of finite elements, i.e. $\sigma_{ij}^{(k)}$ values from solution of boundary value problem equate to net-stress $(\sigma_{ij}^{\text{net}})^{(k)} = \dfrac{\sigma_{ij}^{(k)}}{1 - \rho_s^{(k)}}$.

The following according to [2] are used as criteria of the limiting state of brittle-tough fracture in volume of given finite element:

$$\begin{aligned} &\sigma_1 > S_c \text{ — brittle fracture;} \\ &\kappa_k > \varepsilon_{\text{cr}}^{(k)}\left(\frac{\sigma_m}{\sigma_i}\right) \text{ — tough fracture,} \end{aligned} \qquad (12)$$

where σ_1 is the maximum main net-stress; $\kappa_k = \int d\varepsilon_i^p = \sum_k (d\varepsilon_i^p)^{(k)}$ is the Odqvist parameter of strain hardening; $\varepsilon_{\text{cr}}^{(k)}$ is the critical value κ_k in k-th tracing step depending on rigidity of stressed state.

For example, based on MacKenzie [2]

$$\varepsilon_{\text{cr}}^{(k)}\left(\frac{\sigma_m}{\sigma_i}\right) > \varepsilon_0 + a \exp\left(-1.5\,\frac{\sigma_m^{(k)}}{\sigma_i^{(k)}}\right), \qquad (13)$$

where ε_0 and a are the experimental characteristics of materials (for hull steels $\varepsilon_0 = 0.07$, $a = 2.99$).

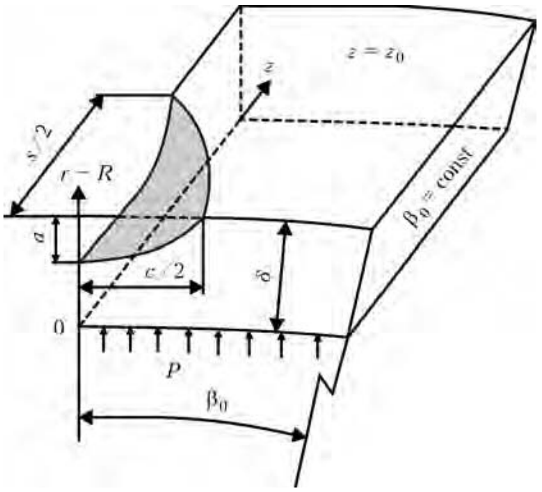

Figure 1. Scheme of fragment of pipe casing with defect of thinning being loaded by internal pressure P on the surface $r - R = 0$ and nominal stresses $\sigma_{\beta\beta}$, $\sigma_{\beta z}$ in plain $\beta = \beta_0$ and σ_{zz}, σ_{zr} in plain $z = z_0$ and symmetry conditions $\beta = 0$, $z = 0$

Method of accumulation of tough fractures in the volume of given element can be used according to [2] in the next form for the case of rapid change in tracing of $(\sigma_m/\sigma_i)^{(k)}$ and $\varepsilon_{\text{cr}}^{(k)}$ values respectively:

$$\sum_{k=0}^{k_{\text{cr}}} \left(\frac{\Delta\varepsilon_i^p}{\kappa}\right)_k = 1, \qquad (14)$$

where k_{cr} is the limiting value of tracing step at which given finite element will «fail», i.e. its mechanical properties rapidly change for properties of air or corresponding aggressive liquid (in presence of respective access).

Present procedure at this step of tracing on loading is performed in iteration way with constant external loading since such a replacement of properties results in redistribution of loads in adjacent finite elements. The case when replacement procedure in the given finite element leads during the next iteration to the replacements in the adjacent elements up to «spontaneous fracture» (when replacement procedure covers large volume of considered structure at specified loading) is quite natural at that. Corresponding conditions for coming of such a state are considered as macroconditions of coming of the limiting state.

Described approach is to be applied to steel pressure vessel with defect overall dimensions $s \times c \times a$ (Figure 1), where s — dimension along the generatrix; c — along the circumference; a — same to depth of the wall in which the thinning was found. Elastic characteristics of steel E and ν, yield strength σ_y and index of power strain hardening m are known.

Estimation of limiting pressure P_{lim}, at which macroscopic spontaneous fracture of the wall takes place in zone of thinning, is necessary under conditions of three-axial stressed state with internal pressure P.

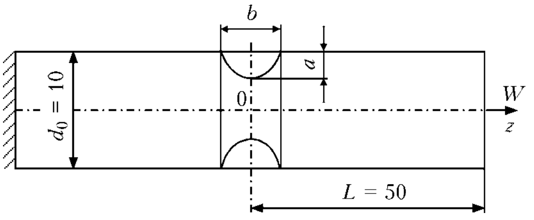

Figure 2. Scheme of axisymmetric notched cylinder specimen of $a \times b$ dimensions

Algorithm of numerical determination in scope of 3D stress-strain state in zone of considered defect taking no account to porosity is given in work [6]. The latter was considered in this work using equations (1)–(14).

Necessary data for such a model connected with specified steel are proposed to be determined using simple tensile experiments of axisymmetric notched cylinder specimens (Figure 2) from pipe steel with yield strength $\sigma_y \approx 480$ MPa. Two dimensions of notch in 10 mm diameter specimens were considered. The first is $a \times b = 1 \times 3$ and the second is $a \times b = 3 \times 1$ mm at theoretical concentration factors $\alpha_{\text{theor}} = 1.60$ and 3.45.

$\sigma_{zz}^{\text{lim}} = 500$ and 130 MPa are the corresponding average fracture axial stresses on clamps. For these data the process of loading of the specimens was simulated at different variation of initial data (Table 1) responsible for pore formation (Figure 3). At that variants 1–10 correspond to predetermined loading on the clamps (section $z = L$) and variant 11 — to predetermined value of axial movement $W = \Delta W n$, where n is the loading step.

Table 1. Variants of initial data responsible for pore formation

Number of variant	σ_y, MPa	ρ_V	S_c, MPa	m
1	480	0.07	1000	0.14
2	480	0.05	1000	0.14
3	480	0.03	1000	0.14
4	480	0	1000	0.14
5	400	0.05	1000	0.14
6	300	0.05	1000	0.14
7	480	0.05	1000	0.05
8	480	0.05	1000	0.25
9	480	0.05	700	0.14
10	480	0.05	1500	0.14
11	480	0.05	1000	0.14

Note. $(\varepsilon_i^p)_0 = 0.01$.

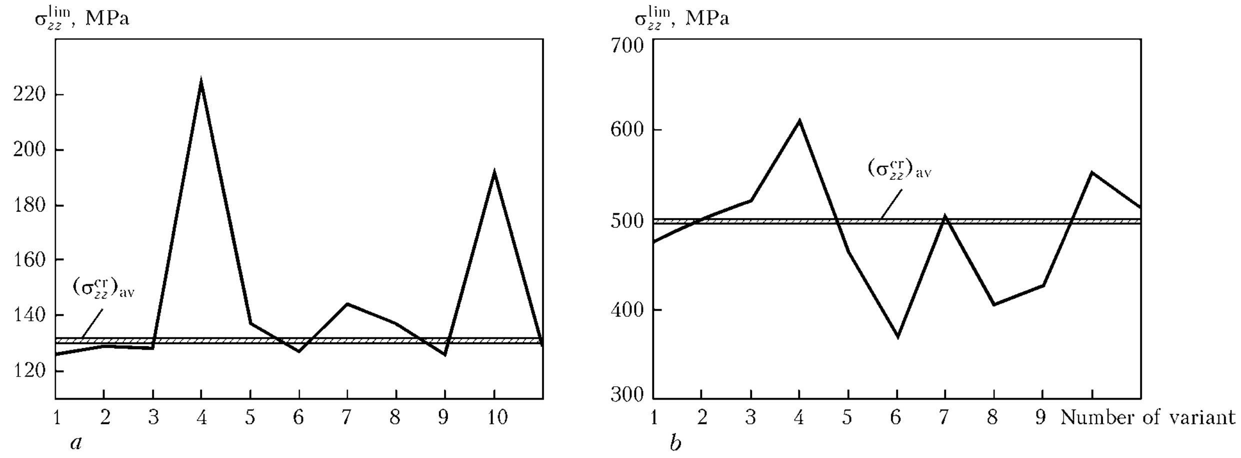

Figure 3. Results of computer simulation of the nominal limiting stresses σ_{zz}^{lim} in section $z = L$ and spontaneous fracture in section $z = 0$ of notched specimen of $a \times b = 3 \times 1$ (a) and 1×3 (b) dimensions ($\alpha_{\text{theor}} = 3.45$) for different variants of change of σ_y, ρ_V, S_c, m (Table 1) in comparison with experimental data on $(\sigma_{zz}^{\text{cr}})_{\text{av}}$ (σ_{zz} is set at $z = L$ for variants 1–10; increment $\Delta W = 0.00261$ mm is set per each step for variant 11)

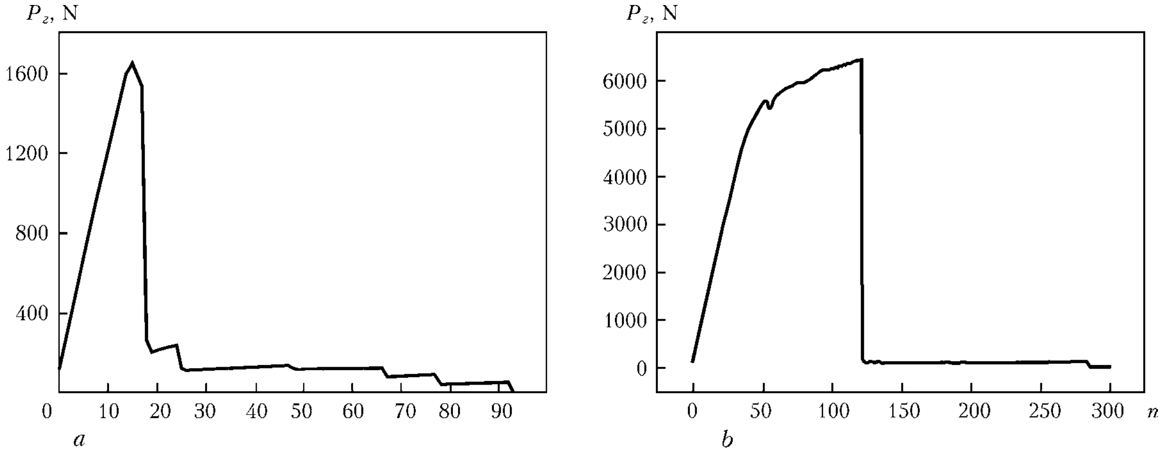

Figure 4. Results of simulation of load P_z on the edge $z = L = 50$ mm for notched specimen of $a \times b = 3 \times 1$ (a) and 1×3 (b) mm dimensions depending on step n at $\Delta W = 0.00261$ mm

Table 2. Initial and calculation data for considered wall thinning defects (c = 40 mm, a = 14 mm)

Number of variant	s, mm	$[P]$, MPa	P_{lim}, MPa	n_{saf}
1	66	7.50	18.8	2.5
2	100	5.15	17.4	3.3
3	200	4.15	14.0	3.2

For this case Figure 4 shows the kinetics of load change P_z in the process of n value growth up to coming of spontaneous fracture (without further increase of load P_z).

Correlation of σ_{zz}^{lim} value with specified average value shows that taking no account to porosity (variant 4 in Figure 3) provides conservative values of σ_{zz}^{lim}. At the same time reduction of σ_y below 300 MPa or S_c below 700 MPa as well as increase of m significantly reduce σ_{zz}^{lim} value. Change of porosity ρ_V (the main factor of fracture zone embrittlement) in the range of $\rho_V \approx \approx 0.03$–$0.07$ provides insignificant effect on σ_{zz}^{lim} critical value.

Fracture process taking into account pore formation which promotes embrittlement of the fracture zone has sufficiently high resistance to main parameters of the considered model (ρ_V, S_c, σ_y, m) for steel under study from this analysis. This allows using their approximate values for practical estimations.

ρ_V = 0.05, S_c = 1000 MPa, σ_y = 440 MPa, m = 0.14 and $(\varepsilon_i^p)_0$ = 0.01 were used in accordance with indicated for determination of critical load in the zone of local thinning of the wall of casing of $2R$ = 1420 mm diameter pipe at wall thickness δ = 20 mm from steel under consideration at 3D analysis.

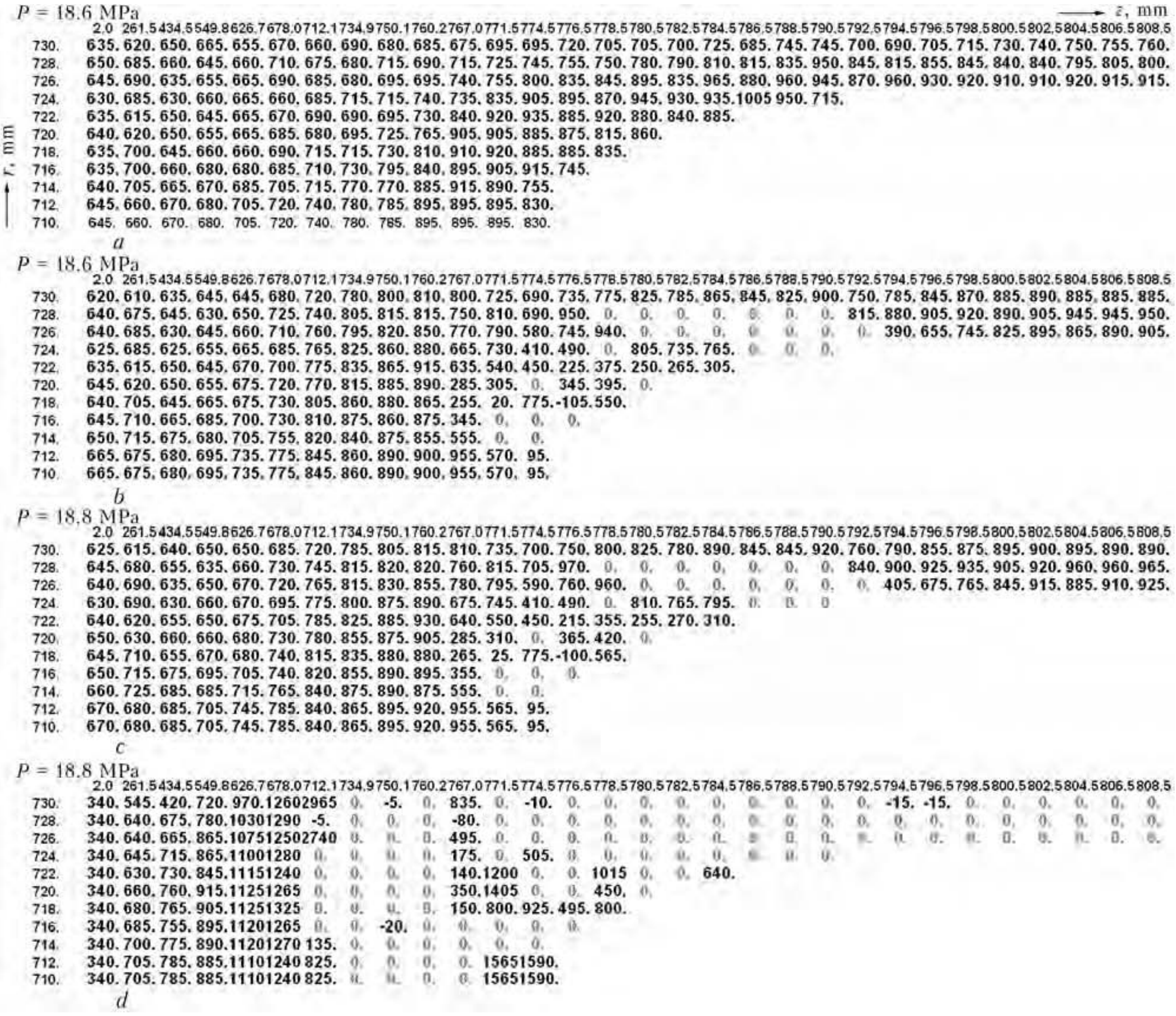

```
P = 18.6 MPa
       2.0 261.5434.5549.8626.7678.0712.1734.9750.1760.2767.0771.5774.5776.5778.5780.5782.5784.5786.5788.5790.5792.5794.5796.5798.5800.5802.5804.5806.5808.5
730.   635. 620. 650. 665. 655. 670. 660. 690. 680. 685. 675. 695. 695. 720. 705. 705. 700. 725. 685. 745. 745. 700. 690. 705. 715. 730. 740. 750. 755. 760.
728.   650. 685. 660. 645. 660. 710. 675. 680. 715. 690. 715. 725. 745. 755. 750. 780. 790. 810. 815. 835. 950. 845. 815. 855. 845. 840. 840. 795. 805. 800.
726.   645. 690. 635. 655. 665. 690. 685. 680. 695. 695. 740. 755. 800. 835. 845. 895. 835. 965. 880. 960. 945. 870. 960. 930. 920. 910. 910. 920. 915. 915.
724.   630. 685. 630. 660. 665. 660. 685. 715. 715. 740. 735. 835. 905. 895. 870. 945. 930. 935.1005 950. 715.
722.   635. 615. 650. 645. 665. 670. 690. 690. 695. 730. 840. 920. 935. 885. 920. 880. 840. 885.
720.   640. 620. 650. 655. 665. 685. 680. 695. 725. 765. 905. 905. 885. 875. 815. 860.
718.   635. 700. 645. 660. 660. 690. 715. 715. 730. 810. 910. 920. 885. 885. 835.
716.   635. 700. 660. 680. 680. 685. 710. 730. 795. 840. 895. 905. 915. 745.
714.   640. 705. 665. 670. 685. 705. 715. 770. 770. 885. 915. 890. 755.
712.   645. 660. 670. 680. 705. 720. 740. 780. 785. 895. 895. 895. 830.
710.   645. 660. 670. 680. 705. 720. 740. 780. 785. 895. 895. 895. 830.
                      a
P = 18.6 MPa
       2.0 261.5434.5549.8626.7678.0712.1734.9750.1760.2767.0771.5774.5776.5778.5780.5782.5784.5786.5788.5790.5792.5794.5796.5798.5800.5802.5804.5806.5808.5
730.   620. 610. 635. 645. 645. 680. 720. 780. 800. 810. 800. 725. 690. 735. 775. 825. 785. 865. 845. 825. 900. 750. 785. 845. 870. 885. 890. 885. 885. 885.
728.   640. 675. 645. 630. 650. 725. 740. 805. 815. 815. 750. 810. 690. 950.   0.   0.   0.   0.   0.   0.   0. 815. 880. 905. 920. 890. 905. 945. 945. 950.
726.   640. 685. 630. 645. 660. 710. 760. 795. 820. 850. 770. 790. 580. 745. 940.   0.   0.   0.   0.   0.   0.   0. 390. 655. 745. 825. 895. 865. 890. 905.
724.   625. 685. 625. 655. 665. 685. 765. 825. 860. 880. 665. 730. 410. 490.   0. 805. 735. 765.   0.   0.   0.
722.   635. 615. 650. 645. 670. 700. 775. 835. 865. 915. 635. 540. 450. 225. 375. 250. 265. 305.
720.   645. 620. 650. 655. 675. 720. 770. 815. 885. 890. 285. 305.   0. 345. 395.   0.
718.   640. 705. 645. 665. 675. 730. 805. 860. 880. 865. 255.  20. 775.-105.550.
716.   645. 710. 665. 685. 700. 730. 810. 875. 860. 875. 345.   0.   0.   0.
714.   650. 715. 675. 680. 705. 755. 820. 840. 875. 855. 555.   0.   0.
712.   665. 675. 680. 695. 735. 775. 845. 860. 890. 900. 955. 570.  95.
710.   665. 675. 680. 695. 735. 775. 845. 860. 890. 900. 955. 570.  95.
                      b
P = 18.8 MPa
       2.0 261.5434.5549.8626.7678.0712.1734.9750.1760.2767.0771.5774.5776.5778.5780.5782.5784.5786.5788.5790.5792.5794.5796.5798.5800.5802.5804.5806.5808.5
730.   625. 615. 640. 650. 650. 685. 720. 785. 805. 815. 810. 735. 700. 750. 800. 825. 780. 890. 845. 845. 920. 760. 790. 855. 875. 895. 900. 895. 890. 890.
728.   645. 680. 655. 635. 660. 730. 745. 815. 820. 820. 760. 815. 705. 970.   0.   0.   0.   0.   0.   0.   0. 840. 900. 925. 935. 905. 920. 960. 960. 965.
726.   640. 690. 635. 650. 670. 720. 765. 815. 830. 855. 780. 795. 590. 760. 960.   0.   0.   0.   0.   0.   0.   0. 405. 675. 765. 845. 915. 885. 910. 925.
724.   630. 690. 630. 660. 670. 695. 775. 800. 875. 890. 675. 745. 410. 490.   0. 810. 765. 795.   0.   0.   0
722.   640. 620. 655. 650. 675. 705. 785. 825. 885. 930. 640. 550. 450. 215. 355. 255. 270. 310.
720.   650. 630. 660. 660. 680. 730. 780. 855. 875. 905. 285. 310.   0. 365. 420.   0.
718.   645. 710. 655. 670. 680. 740. 815. 835. 880. 880. 265.  25. 775.-100.565.
716.   650. 715. 675. 695. 705. 740. 820. 855. 890. 895. 355.   0.   0.   0.
714.   660. 725. 685. 685. 715. 765. 840. 875. 890. 875. 555.   0.   0.
712.   670. 680. 685. 705. 745. 785. 840. 865. 895. 920. 955. 565.  95.
710.   670. 680. 685. 705. 745. 785. 840. 865. 895. 920. 955. 565.  95.
                      c
P = 18.8 MPa
       2.0 261.5434.5549.8626.7678.0712.1734.9750.1760.2767.0771.5774.5776.5778.5780.5782.5784.5786.5788.5790.5792.5794.5796.5798.5800.5802.5804.5806.5808.5
730.   340. 545. 420. 720. 970.12602965   0.  -5.   0. 835.   0. -10.   0.   0.   0.   0.   0.   0.   0.   0.   0. -15. -15.   0.   0.   0.   0.   0.   0.   0.
728.   340. 640. 675. 780.10301290  -5.   0.   0.   0. -80.   0.   0.   0.   0.   0.   0.   0.   0.   0.   0.   0.   0.   0.   0.   0.   0.   0.   0.   0.
726.   340. 640. 665. 865.107512502740   0.   0.   0. 495.   0.   0.   0.   0.   0.   0.   0.   0.   0.   0.   0.   0.   0.   0.   0.   0.   0.   0.   0.
724.   340. 645. 715. 865.11001280   0.   0.   0.   0. 175.   0. 505.   0.   0.   0.   0.   0.   0.   0.   0.
722.   340. 630. 730. 845.11151240   0.   0.   0.   0. 140.1200   0.   0. 1015   0.   0. 640.
720.   340. 660. 760. 915.11251265   0.   0.   0.   0. 350.1405   0.   0. 450.   0.
718.   340. 680. 765. 905.11251325   0.   0.   0.   0. 150. 800. 925. 495. 800.
716.   340. 685. 755. 895.11201265   0.   0. -20.   0.   0.   0.   0.   0.
714.   340. 700. 775. 890.11201270 135.   0.   0.   0.   0.   0.   0.
712.   340. 705. 785. 885.11101240 825.   0.   0.   0.   0. 15651590.
710.   340. 705. 785. 885.11101240 825.   0.   0.   0.   0. 15651590.
                      d
```

Figure 5. Distribution of main stresses σ_1 in the longitudinal section β = 0 at various internal pressure: a, b — P = = 18.6 MPa during the first (a) and the last (b) iteration; c, d — P = 18.8 MPa during the first iteration (c) and the last (d) (zeros indicate the finite elements where fracture takes place)

$P = 18.6$ MPa

$\longrightarrow z$, mm

$\uparrow r$, mm

	2.0	261.5	434.5	549.8	626.7	678.0	712.1	734.9	750.1	760.2	767.0	771.5	774.5	776.5	778.5	780.5	782.5	784.5	786.5	788.5	790.5	792.5	794.5	796.5	798.5	800.5	802.5	804.5	806.5	808.5
730.	0.021	0.020	0.024	0.028	0.029	0.031	0.033	0.037	0.041	0.044	0.048	0.049	0.049	0.050	0.051	0.052	0.054	0.054	0.058	0.060	0.063	0.072	0.076	0.077	0.078	0.079	0.081	0.082	0.083	0.083
728.	0.022	0.020	0.025	0.029	0.031	0.033	0.037	0.042	0.047	0.054	0.060	0.067	0.072	0.077	0.083	0.089	0.098	0.102	0.115	0.126	0.126	0.149	0.144	0.140	0.137	0.136	0.135	0.132	0.132	0.132
726.	0.024	0.022	0.026	0.031	0.033	0.036	0.041	0.047	0.055	0.065	0.075	0.085	0.096	0.105	0.115	0.126	0.145	0.147	0.173	0.190	0.217	0.242	0.215	0.208	0.200	0.194	0.189	0.183	0.181	0.181
724.	0.026	0.023	0.028	0.032	0.036	0.039	0.045	0.052	0.062	0.075	0.089	0.103	0.117	0.130	0.147	0.158	0.184	0.198	0.227	0.251	0.290									
722.	0.027	0.025	0.029	0.033	0.037	0.042	0.049	0.057	0.070	0.085	0.102	0.120	0.137	0.153	0.169	0.184	0.197	0.185												
720.	0.028	0.026	0.030	0.035	0.040	0.045	0.053	0.063	0.077	0.094	0.115	0.137	0.156	0.168	0.178	0.170														
718.	0.030	0.027	0.031	0.036	0.042	0.047	0.058	0.068	0.083	0.104	0.128	0.153	0.173	0.183	0.173															
716.	0.031	0.028	0.032	0.038	0.045	0.051	0.061	0.073	0.090	0.112	0.140	0.168	0.192	0.209																
714.	0.033	0.030	0.033	0.039	0.047	0.054	0.065	0.078	0.097	0.118	0.150	0.183	0.223																	
712.	0.035	0.032	0.034	0.042	0.049	0.057	0.068	0.085	0.104	0.125	0.156	0.185	0.200																	
710.	0.035	0.032	0.034	0.042	0.049	0.057	0.068	0.085	0.104	0.125	0.156	0.185	0.200																	

a

$P = 18.6$ MPa

	2.0	261.5	434.5	549.8	626.7	678.0	712.1	734.9	750.1	760.2	767.0	771.5	774.5	776.5	778.5	780.5	782.5	784.5	786.5	788.5	790.5	792.5	794.5	796.5	798.5	800.5	802.5	804.5	806.5	808.5
730.	0.021	0.020	0.024	0.028	0.029	0.031	0.033	0.038	0.043	0.049	0.056	0.062	0.066	0.069	0.072	0.077	0.084	0.084	0.088	0.090	0.091	0.097	0.097	0.097	0.097	0.097	0.098	0.099	0.100	0.100
728.	0.022	0.020	0.025	0.029	0.031	0.033	0.037	0.043	0.050	0.059	0.071	0.082	0.091	0.096	0.	0.	0.	0.	0.	0.	0.	0.181	0.162	0.157	0.154	0.152	0.151	0.148	0.148	0.148
726.	0.024	0.022	0.026	0.031	0.033	0.036	0.041	0.048	0.058	0.071	0.086	0.101	0.111	0.119	0.131	0.	0.	0.	0.	0.	0.	0.	0.215	0.215	0.210	0.205	0.201	0.195	0.193	0.193
724.	0.026	0.023	0.028	0.032	0.035	0.039	0.045	0.054	0.065	0.081	0.099	0.118	0.121	0.131	0.	0.158	0.198	0.214	0.	0.	0.									
722.	0.027	0.025	0.029	0.033	0.037	0.042	0.049	0.059	0.073	0.091	0.109	0.135	0.138	0.154	0.170	0.192	0.197	0.185												
720.	0.028	0.026	0.030	0.035	0.040	0.045	0.053	0.065	0.081	0.100	0.117	0.148	0.	0.179	0.188	0.														
718.	0.030	0.027	0.031	0.036	0.042	0.047	0.058	0.070	0.087	0.109	0.129	0.166	0.228	0.245	0.176															
716.	0.031	0.028	0.032	0.038	0.045	0.051	0.061	0.075	0.094	0.118	0.143	0.	0.	0.																
714.	0.033	0.030	0.033	0.039	0.047	0.054	0.065	0.080	0.101	0.124	0.163	0.	0.																	
712.	0.035	0.032	0.034	0.042	0.049	0.057	0.068	0.086	0.107	0.131	0.174	0.190	0.206																	
710.	0.035	0.032	0.034	0.042	0.049	0.057	0.068	0.086	0.107	0.131	0.174	0.190	0.206																	

b

$P = 18.8$ MPa

$\longrightarrow z$, mm

	2.0	261.5	434.5	549.8	626.7	678.0	712.1	734.9	750.1	760.2	767.0	771.5	774.5	776.5	778.5	780.5	782.5	784.5	786.5	788.5	790.5	792.5	794.5	796.5	798.5	800.5	802.5	804.5	806.5	808.5
730.	0.021	0.020	0.024	0.028	0.029	0.031	0.033	0.038	0.043	0.049	0.056	0.062	0.066	0.069	0.072	0.078	0.084	0.084	0.088	0.090	0.091	0.097	0.097	0.097	0.097	0.097	0.098	0.099	0.100	0.100
728.	0.022	0.020	0.025	0.029	0.031	0.033	0.037	0.043	0.050	0.059	0.071	0.082	0.091	0.096	0.	0.	0.	0.	0.	0.	0.	0.181	0.162	0.157	0.154	0.152	0.151	0.148	0.148	0.148
726.	0.024	0.022	0.026	0.031	0.033	0.036	0.041	0.048	0.058	0.071	0.086	0.101	0.111	0.119	0.131	0.	0.	0.	0.	0.	0.	0.	0.215	0.215	0.210	0.205	0.201	0.195	0.193	0.193
724.	0.026	0.023	0.028	0.032	0.035	0.039	0.045	0.054	0.065	0.081	0.099	0.118	0.121	0.131	0.	0.158	0.198	0.214	0.	0.	0.									
722.	0.027	0.025	0.029	0.033	0.037	0.042	0.049	0.059	0.073	0.091	0.109	0.135	0.138	0.154	0.170	0.192	0.197	0.185												
720.	0.028	0.026	0.030	0.035	0.040	0.045	0.053	0.065	0.081	0.100	0.117	0.148	0.	0.179	0.188	0.														
718.	0.030	0.027	0.031	0.036	0.042	0.047	0.058	0.070	0.087	0.109	0.129	0.166	0.228	0.245	0.176															
716.	0.031	0.028	0.032	0.038	0.045	0.051	0.061	0.075	0.094	0.118	0.143	0.	0.	0.																
714.	0.033	0.030	0.033	0.039	0.047	0.054	0.065	0.080	0.101	0.124	0.163	0	0																	
712.	0.035	0.032	0.034	0.042	0.049	0.057	0.068	0.086	0.107	0.131	0.175	0.190	0.206																	
710.	0.035	0.032	0.034	0.042	0.049	0.057	0.068	0.086	0.107	0.131	0.175	0.190	0.206																	

c

$P = 18.8$ MPa

	2.0	261.5	434.5	549.8	626.7	678.0	712.1	734.9	750.1	760.2	767.0	771.5	774.5	776.5	778.5	780.5	782.5	784.5	786.5	788.5	790.5	792.5	794.5	796.5	798.5	800.5	802.5	804.5	806.5	808.5
730.	0.049	0.020	0.024	0.052	0.351	1.750	50.50	0.	0.157	0	0.299	0.	0.332	0.	0.	0.	0.	0.	0.	0.	0.	0.	0.234	0.234	0.	0.	0.	0.	0.	0.
728.	0.049	0.021	0.026	0.064	0.373	1.727	0.205	0.	0.	0	5.557	0.	0.	0.	0.	0.	0.	0.	0.	0.	0.	0.	0.	0.	0.	0.	0.	0.	0.	0.
726.	0.051	0.022	0.031	0.077	0.401	1.717	36.10	0.	0.	0.	4.207	0.	0.	0.	0.	0.	0.	0.	0.	0.	0.	0.	0.	0.	0.	0.	0.	0.	0.	0.
724.	0.052	0.024	0.035	0.090	0.430	1.702	0.	0	0	0	3.950	0.	0.206	0	0.	0.	0.	0.	0.	0.	0.									
722.	0.054	0.026	0.039	0.103	0.462	1.684	0.	0.	0.	0.	2.917	1.937	0.	0.	1.282	0.	0.	0.301												
720.	0.055	0.028	0.043	0.116	0.496	1.641	0.	0.	0.	0.	3.177	1.612	0.	0.	0.194	0.														
718.	0.056	0.029	0.047	0.130	0.532	1.543	0.	0.	0.	0.	0.134	0.892	0.533	0.279	0.325															
716.	0.057	0.031	0.052	0.144	0.570	1.499	0.	0.	12.18	0.	0.	0.	0.	0.																
714.	0.059	0.033	0.056	0.157	0.607	1.444	0.200	0.	0.	0.	0.	0.	0.																	
712.	0.061	0.036	0.060	0.173	0.644	1.410	0.220	0.	0.	0.	0.	14.03	22.403																	
710.	0.061	0.036	0.060	0.173	0.644	1.410	0.220	0.	0.	0	0.	14.03	22.403																	

d

Figure 6. The same as in Figure 5 but for $\kappa_k = \int d\varepsilon_i^p = \sum (d\varepsilon_i^p)^{(k)}$ value

Three variants of geometrical defects from Table 2 were studied. The Table shows the results of calculation of allowable pressures $[P]$ for considered thinning defects. Figures 5 and 6 illustrate the result of calculation of the limiting pressure at which spontaneous fracture takes place for variant 1. Similar data are given for variants 2 and 3. Respectively, Table 2 also shows information about limiting P_{lim} and safety factors $n_{\text{saf}} = P_{\text{lim}}/[P]$.

Matching of calculation limiting loads on the results of given work, i.e. considering pore formation, with calculation allowable loads from work [7], obtained based on broad experiment, related with fracture of full-scale specimens through the safety factor in the range of $n_{\text{saf}} = 2.0$–2.5, shows their good compliance.

CONCLUSIONS

1. Mathematical modelling of the limiting state for steel pressure vessels involving geometrical defects of wall thinning requires more general models for description of not only deformation process (for example, considering larger deformation), but fracture process as well after developed plastic flow stage (for example, pore formation).

2. It is shown that the attraction of sufficiently known physical models of pore formation at plastic flow results in certain «embrittlement» effect of fracture zone at that sufficiently reducing the limiting calculation loading (per 20–70 % and more).

3. The results of matching of limiting calculation loads from Table 2 on procedure of this study with that allowable on work [7] based on the broad experiment show that the safety factor $n_{\text{saf}} \approx 2.0$–$2.5$ specified at that has good enough correspondence with data of Table 2 as a rule.

1. Romanova, V.A. (2008) *Modeling of deformation and fracture processes in three-dimensional structur-*

ally heterogeneous materials: Syn. of Thesis for Dr. of Techn. Sci. Degree. Tomsk.
2. Karzov, G.P., Margolin, B.Z., Shvetsova, V.A. (1993) *Physical-mechanical modeling of fracture processes*. St.-Petersburg: Politekhnika.
3. Rybin, V.V. (1986) *High plastic strains and fracture of metals*. Moscow: Metallurgiya.
4. (1986) *Static strength and fracture mechanics of steels*. Ed. by V. Dal, V. Antonov. Moscow: Metallurgizdat.
5. Makhnenko, V.I. (1976) *Computational methods for investigation of kinetics of welding stresses and strains*. Kiev: Naukova Dumka.
6. Makhnenko, V.I., Velikoivanenko, O.A., Pozynka, G.P. et al. (2009) Stressed state in zone of thinning defects of thin-wall pipes. In: *Problems of service life and service safety of structures, buildings and machines*. Ed. by B.E. Paton. Kyiv: PWI.
7. (2000) *Fitness-for-service*: American Petroleum Institute recommended practice 579. 1st ed.

INFLUENCE OF WELDING THERMAL CYCLE ON STRUCTURE AND PROPERTIES OF MICROALLOYED STRUCTURAL STEELS

V.A. KOSTIN, G.M. GRIGORENKO, V.D. POZNYAKOV, S.L. ZHDANOV, T.G. SOLOMIJCHUK, T.A. ZUBER and **A.A. MAKSIMENKO**
E.O. Paton Electric Welding Institute, NASU, Kiev, Ukraine

Influence of welding thermal cycle on microstructure and properties of HAZ metal in new steels with carbide and carbonitride type of strengthening, namely 06GBD, 10G2FB, 15KSATYuD, was studied. It is shown that under the influence of welding thermal cycle an optimum complex of ferritic-bainitic structures forms in a rather broad range of cooling rates ($w_{6/5}$ = 10–30 °C/s), which is characterized by values of strength, ductility and cold resistance on the level of requirements made of base metal of strength class C440.

Keywords: *arc welding, structural steels, carbonitride strengthening, welding thermal cycle, Gleeble 3800, microstructure, bainite, MAC-phase, mechanical properties*

At present transportation engineering and building industry of Ukraine are the main users of higher strength steels with yield point of up to 400 MPa. Today, however, they no longer satisfy, by a number of objective factors, the requirements of high-speed traffic or modern concepts of urban planning, both by the level of strength and impact toughness.

Over the recent years, PWI in cooperation with metallurgists developed a number of new steels with 440–590 MPa yield point, based on the principle of carbide and carbonitride strengthening [1, 2].

As welding is the main technological process of fabrication of structures from these steels, improved performance of the new steels (by strength and impact toughness level) should be preserved also in the welded joints. However, HAZ formation in the metal being welded leads to deterioration of mechanical properties under the impact of welding thermal cycle (WTC), both as a result of grain growth, and in connection with formation of quenching structures. Wide introduction of new steels should be preceded by profound comprehensive investigation of these steels reaction to WTC.

Disembodied published data on the features of structural changes in the new steels with carbide and carbonitride strengthening under WTC conditions are obviously insufficient [3, 4].

In addition, the clearly increased requirements to impact toughness of new steels of strength class C345–440 (KCU_{-40} = 39 J/cm^2, KCU_{-70} = 34 J/cm^2 to GOST 27772–88) require studying WTC effect on strength and impact toughness levels in HAZ metal.

The objective of this work consisted in investigation of the features of formation of HAZ metal structure under WTC impact and assessment of microstructure influence on mechanical properties and impact toughness in this zone, in order to select optimum welding modes, ensuring high performance of the welded joint.

Table 1 gives the composition of the studied steel grades. Steels 10G2FB and 06GBD belong to steels with carbide strengthening type, and 15KhSATYuD steel is of carbonitride strengthening type. Mechanical properties of steels in as-delivered condition are given in Tables 2 and 3.

In order to evaluate WTC effect on the structure of welded joint HAZ metal, investigations were conducted on model samples in Geeble 3800